THE FASEB JOURNAL • RESEARCH • www.fasebj.org

Inositol polyphosphate multikinase is a metformin target that regulates cell migration

Becky Tu-Sekine,* Abinash Padhi,† Sunghee Jin,* Srivathsan Kalyan,‡ Karanpreet Singh,§ Matthew Apperson,† Rakesh Kapania,§ Soojung Claire Hur,‡ Amrinder Nain,† and Sangwon F. Kim*,[1]

*Department of Medicine, Division of Endocrinology, Diabetes, and Metabolism, and ‡Department of Mechanical Engineering, Johns Hopkins University, Baltimore, Maryland, USA; and †Department of Mechanical Engineering and §Department of Aerospace and Ocean Engineering, Virginia Tech, Blacksburg, Virginia, USA

ABSTRACT: Metformin has been shown to alter cell adhesion protein expression, which is thought to play a role in its observed antitumor properties. We found that metformin treatment down-regulated integrin β1 concomitant with the loss of inositol polyphosphate multikinase (IPMK) in murine myocytes, adipocytes, and hepatocytes. To determine if IPMK was upstream of integrin β1 expression, we examined IPMK$^{-/-}$ mouse embryonic fibroblast cells and found that integrins β1 and β3 gene expression was reduced by half, relative to wild-type cells, whereas focal adhesion kinase (FAK) activity and Rho/Rac/Cdc42 protein levels were increased, resulting in migration defects. Using nanonet force microscopy, we determined that cell:extracellular matrix adhesion and cell contractility forces were decreased, confirming the functional relevance of integrin and Rho protein dysregulation. Pharmacological studies showed that inhibition of both FAK1 and proline-rich tyrosine kinase 2 partially restored integrin β1 expression, suggesting negative regulation of integrin β1 by FAK. Together our data indicate that IPMK participates in the regulation of cell migration and provides a potential link between metformin and wound healing impairment.—Tu-Sekine, B., Padhi, A., Jin, S., Kalyan, S., Singh, K., Apperson, M., Kapania, R., Hur, S. C., Nain, A., Kim, S. F. Inositol polyphosphate multikinase is a metformin target that regulates cell migration. FASEB J. 33, 000–000 (2019). www.fasebj.org

KEY WORDS: integrin · adhesion · focal adhesion kinase · nanonet force microscopy · extracellular matrix

Metformin, the most prescribed antidiabetic, is a well-studied regulator of energy homeostasis that inhibits gluco neogenesis and increases insulin sensitivity through AMPK-dependent and independent pathways. We and others have shown that inositol polyphosphate multikinase (IPMK) participates in energy homeostasis and amino acid sensing through protein-protein interactions with AMPK (AMP-dependent kinase), liver kinase B1(LKB1), and mammalian target of rapamycin C1 (mTORC1), and we have previously observed that IPMK levels are modulated in response to energy stress, implicating IPMK in the metformin response (1–4). More recently, metformin has been shown to inhibit tumorigenesis in glioblastoma, breast cancer, and prostate cancer cell lines, in part by decreasing cell migration. Although the mechanism of compromised migration is not well defined, numerous studies report metformin-induced alterations in the expression of proteins involved in cellular adhesion including intercellular adhesion molecule 1 (5), cadherins (6, 7), matrix metalloprotease-9 and -2 (8), and integrins (9), and multiple studies now report an inhibitory effect of metformin on wound healing (10, 11).

Cellular adhesion depends upon a complex interplay between environmental cues and intracellular signaling that ultimately determines the ability of cells to migrate and respond to changes in the extracellular matrix (ECM). Cell migration is a highly orchestrated cascade of events that begins with sensing the environment through filopodial protrusions, followed by cell polarization through formation of stable adhesions in the lamellipodia that establish the actomyosin-based contractile tensional forces necessary for the translocation of the cell body (12). Many physiologic processes require cells to alter cell:ECM or cell:cell adhesion to control cell migration; this process is key not only to successful wound healing but also embryonic development, metastasis, and differentiation (13). Inositol pyrophosphates such as 5-diphosphoinositol

ABBREVIATIONS: 2D, 2-dimensional; DiPer, directional persistence; ECM, extracellular matrix; FAK, focal adhesion kinase; GFP, green fluorescence protein; IP, inorganic polyphosphate; IPMK, inositol polyphosphate multikinase; MEF, mouse embryonic fibroblast; NFM, nanonet force microscopy; PIP_2, phosphatidylinositol 4,5-bisphosphate; PIP_3, phosphatidylinositol 3,4,5-bisphosphate

[1] Correspondence: Department of Endocrinology, Diabetes and Metabolism, Johns Hopkins University, 5501 Hopkins Bayview Cir., Allergy and Asthma Center, Room 2A.44, Baltimore, MD 21224, USA. E-mail: skim132@jhmi.edu

doi: 10.1096/fj.201900717RR
This article includes supplemental data. Please visit *http://www.fasebj.org* to obtain this information.

pentakisphosphate have been linked to actin cytoskeletal rearrangements involved in cell migration and invasion (14), whereas phosphoinositides such as phosphatidylinositol 4,5-bisphosphate (PIP_2) and phosphatidylinositol 3,4,5-bisphosphate (PIP_3) are powerfully linked to cell migration (15). PIP_2 is a well-known activator of focal adhesion kinase (FAK) and the Rho GTPase family members, which are essential components of cytoskeletal rearrangements, whereas PIP_3 has been shown to play a critical role in promoting lateral spreading and propagation of branched cellular protrusions that contribute to sideways movement (16).

Integrins are well-studied transmembrane receptors that link the internal actin contractile network to the ECM, acting as a sensor that links cellular signaling to the extracellular environment (17, 18) and contributing to many aspects of cellular behavior, including differentiation, proliferation, and apoptosis as well as adhesion and movement (19, 20). Most mammalian cells express integrin β1, which has the highest capacity for interacting with multiple integrin β isoforms, and this plasticity results in the specific requirement for integrin β1 in varied processes (21). Although integrins are most well known for their role in adhering cells to the extracellular substrate, they are also critical components of large mechanically transduced signaling networks through a variety of interacting kinases, GTPases, and scaffolding proteins. Importantly, integrins β1 and β3 are crucial for multiple steps in wound healing, from platelet aggregation to the migration and proliferation of keratinocytes and fibroblasts that are necessary for successful re-epithelialization and angiogenesis (22).

IPMK is the rate-limiting enzyme in the formation of inositol polyphosphates and an important regulator of the PIP_2/PIP_3 ratio in eukaryotic cells (23). As the only enzyme able to convert inorganic polyphosphate (IP)4 to IP5 and IP6 in mammalian cells, IPMK is also the gatekeeper to the formation of the inositol pyrophosphates, and loss of this enzyme results in the depletion of IP5, IP6, and IP7 as well as an ~50% decreases in PIP_3 in mouse embryonic fibroblasts (MEFs) (2, 24). Targeted disruption of the inositol pathway by global and tissue-specific deletion of inositol phosphate kinases underscores the importance of IPMK not only in energy homeostasis but also in direct and epigenetic regulation of gene transcription (25, 26). In this study, we show that IPMK is down-regulated by metformin treatment, and, by using knockout and recovery experiments, we reveal a novel role for IPMK in cell migration.

MATERIALS AND METHODS

Reagents

Metformin was obtained from Cayman Chemicals (Ann Arbor, MI, USA). PF431,396, PF573,228 were from Selleck Chemicals (Houston, TX, USA). G418 was from Corning (Corning, NY, USA). Fibronectin was from Thermo Fisher Scientific (Waltham, MA, USA). Antibodies are from Cell Signaling Technology (Danvers, MA, USA), except active β1 integrin 9EG7 (BD Biosciences, San Jose, CA, USA), IPMK (Covance, Princeton, NJ, USA), myc (Roche Diagnostics, Indianapolis, IN, USA), and vinculin (Santa Cruz Biotechnology, Dallas, TX, USA). Beta–green fluorescence protein (GFP)-pFB-Neo was a gift from Martin Humphries (Addgene, Cambridge, MA, USA; plasmid 69767; *http://n2t.net/addgene:69767*; RRID:Addgene_69767) (27), and pEGFP-N1 was from Takara Bio USA (Mountain View, CA, USA).

Cell culture and transfections

MEFs {IPMK MEFs (fl/fl) [wild type (WT)], $IPMK^{-/-}$ MEF} (3) were maintained in DMEM with 10% fetal bovine serum and 2 mM L-glutamine (complete medium) at 37°C with a 5% CO_2 atmosphere in a humidified incubator. For nanonet force microscopy (NFM) scaffold experiments, 50 μl of cells at a density of 100,000 cells/ml were seeded on the suspended fibers, and 300 μl of medium was placed around the well to prevent evaporation. After incubation for 2 h to facilitate attachment, the wells were flooded with media. Primary adipocyte precursors were harvested from the inguinal fat pads of $IPMK^{fl/fl}$ mice by collagenase digestion and cultured in (DMEM; Thermo Fisher Scientific) containing 10% fetal bovine serum (MilliporeSigma, Burlington, MA, USA). Subconfluent cells were treated with adenovirus containing either GFP or Cre (Vector Biolabs, Malvern, PA, USA). Upon reaching confluence, cells were differentiated by treatment with 0.5 mM 3-isobutyl-1-methylxanthin, 1 μM dexamethasone, and 167 nM insulin for 2 d, followed by continued culture in 167 nM insulin, which was changed every 2 d thereafter until analysis. Primary hepatocytes were isolated essentially as previously described (28). Transient transfections were completed using Lipofectamine 2000 (Thermo Fisher Scientific) according to the manufacturer's protocol.

Immunoblotting

Samples were lysed in RIPA buffer containing inhibitors and heated at 95°C for 5 min prior to electrophoresis. Proteins were transferred to a 0.2-μm nitrocellulose membrane, blocked with 5% nonfat dry milk, and incubated with primary antibodies at 4°C overnight. Blots were imaged and quantitated using an Odyssey Near-Infrared Scanner (Li-Cor Biosciences, Lincoln, NE, USA).

Microscopy and immunofluorescence

Cells were seeded onto fibronectin-treated dishes or fibers and allowed to adhere for at least 1 h prior to imaging experiments. For immunofluorescence experiments, cells were fixed with 4% paraformaldehyde and permeabilized with 0.1% Triton X-100 prior to blocking and staining. F-actin was stained using rhodamine phalloidin (Santa Cruz Biotechnology). Fiber scaffolds were kept hydrated in PBS during imaging using an Axio Observer Z1 microscope (Carl Zeiss GmbH, Oberkochen, Germany) with a ×40 objective. Cells on 2-dimensional (2D) surfaces were imaged using a Lionheart FX microscope (BioTek Instruments, Winooski, VT, USA) at the indicated magnifications.

Quantitative real-time PCR

Total RNA was isolated from WT or $IPMK^{-/-}$ MEF cells using RNeasy Mini Kit (Qiagen, Hilden, Germany), according to the manufacturer's protocol. Primer sequences are listed in the Supplemental Data. Glyceraldehyde 3-phosphate dehydrogenase mRNA was used as the invariant endogenous control, and melting curve analysis was run to verify specificity of each amplicon.

All reactions were performed in triplicate. The relative amounts of the RNAs were calculated using the comparative threshold cycle method. Primers were as follows: integrin (Int)β1 forward 5′-TGCCAAATCTTGCGGAGAATG-3′, reverse: 5′-CCACAATTTGGCCCTGCTTG-3′, Intβ3 forward 5′-GTCACATTGGCACCGACAACC-3′, reverse 5′-CCACACTCAAAAGTCCCGTTC-3′; IntαV forward 5′-CTTRCTCRCGTRGGARGTTRTTARCCG-3′, reverse 5′-GCTRGTCRAAARTTGRAATRGGTRGGTRG-3′; Intα5 forward 5′-CTTRCTCRCGTRGGARGTTRTTARCCG-3′, reverse 5′-GCTRGTCRAAARTTGRAATRGGTRGGTRG-3′; RhoA forward 5′-AGCTTGTGGTAAGACATGCTTG-3′, reverse 5′-GTGTCCCATAAAGCCAACTCTAC-3′; Rac1 forward 5′-GAGACGGAGCTGTTGGTAAAA-3′, reverse 5′-ATAGGCCCAGATTCACTGGTT-3′; Cdc42 forward 5′-CCCATCGGAATATGTACCAACTG-3′, reverse 5′-CCAAGAGTGTATGGCTCTCCAC-3′; IPMK forward 5′-GAAGGAAGGCGTCTCCAAGTT-3′, reverse 5′-CGCCAAAGTTCTATCGTTTGC-3′.

Nanonet manufacturing

Fiber scaffolds were generated as previously reported (29, 30). For migration and force analysis, fiber scaffolds contained a layer of large-diameter fibers (~2 μm) on top of small-diameter (~250 nm) parallel fibers. For protrusion analysis, scaffolds had large-diameter fibers (~2 μm) base fibers and small-diameter protrusive fibers (~500 nM). The fibers were coated with 4 μg/ml fibronectin for 30 min at 37°C immediately prior to seeding cells.

Velocity and protrusions on nanonet fibers

All fiber measurements were done using AxioVision SE64 software (Carl Zeiss GmbH) and ImageJ (National Institutes of Health, Bethesda, MD, USA). Velocity of cells on fibers was calculated by tracking the centroid of the cells, and protrusion length was measured in ImageJ. Protrusions <5 μm in length were excluded. For velocity and protrusion experiments, cells undergoing division during analysis were excluded.

Velocity and cell tracking in 2D tissue culture plates

Cells were seeded onto fibronectin-coated plates at 10–30% cell density and incubated for a minimum of 2 h to permit full adhesion prior to imaging in a humidified environmental chamber (37°C, 5% CO_2) attached to a Lionheart Fx microscope. Images were preprocessed using Gen5 3.04 software (BioTek Instruments) or Fiji/ImageJ with the MIST stitching and SIFT alignment plugins (31, 32) prior to cell tracking analysis using CellTracker v.1.1 (33). Cells undergoing division were excluded from analysis.

Force experiments (nanonet scaffolds)

The inside-out force calculations were done using a custom program written in MatLab (MathWorks, Natick, MA, USA).

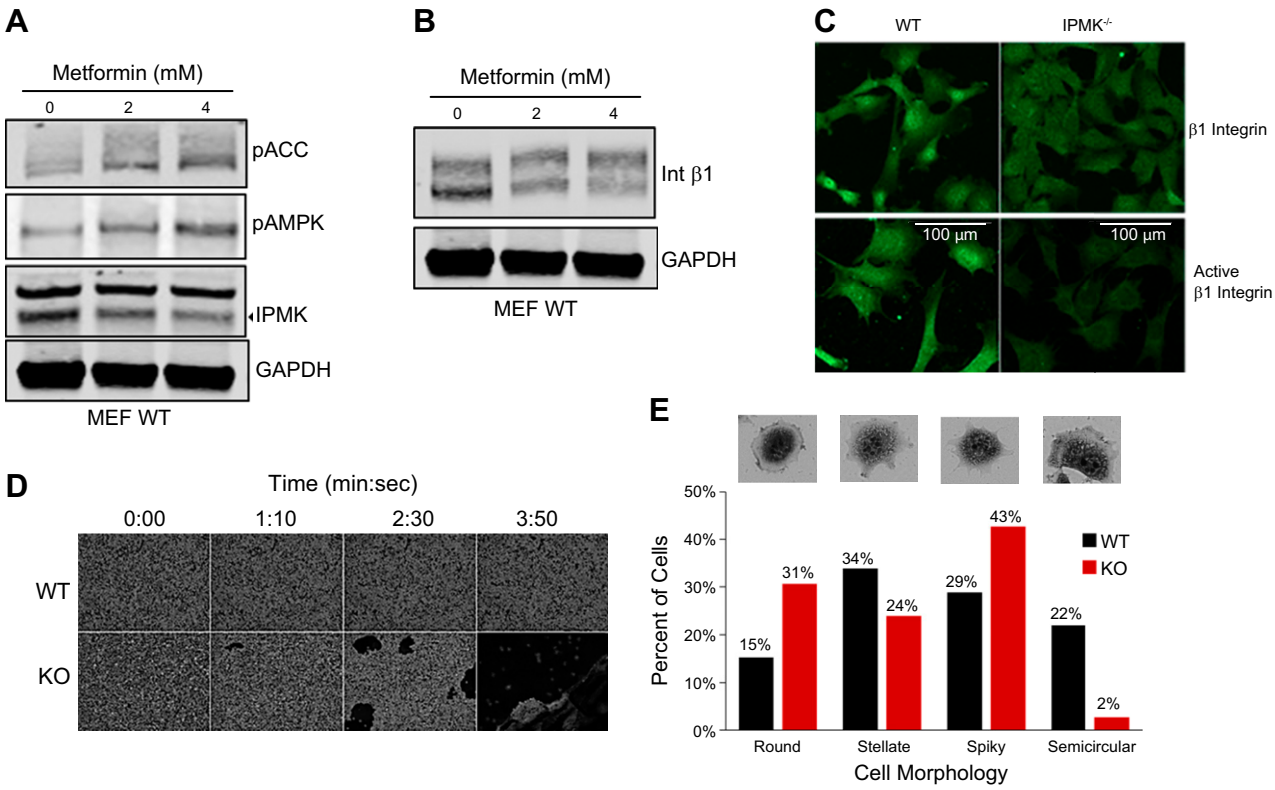

Figure 1. IPMK regulates integrin (Int)β1 expression. *A*, *B*) MEF WT cells were treated with indicated concentration of metformin for 48 h, and cell lysates were subjected to immunoblotting. *C*) Expression of integrin β1 was measured by fluorescence microscopy against total or active form of the integrin β1 protein. Images were taken at ×20 magnification. *D*) MEF (WT *vs.* IPMK$^{-/-}$) cells were washed once with calcium and magnesium-free (CMF) PBS and imaged in CMF PBS every 10 s. *E*) MEF (WT *vs.* IPMK$^{-/-}$) cells were trypsinized briefly and seeded at low density onto fibronectin, allowed to adhere for 1 h, then fixed and stained with Evan's Blue prior to imaging and analysis. Percentages indicate percent of total cells imaged; cells that adhered but did not spread were eliminated from the analysis. The most representative images from 3 independent assays are presented. GAPDH, glyceraldehyde 3-phosphate dehydrogenase; pACC, phosphorylated acetyl-CoA carboxylase.

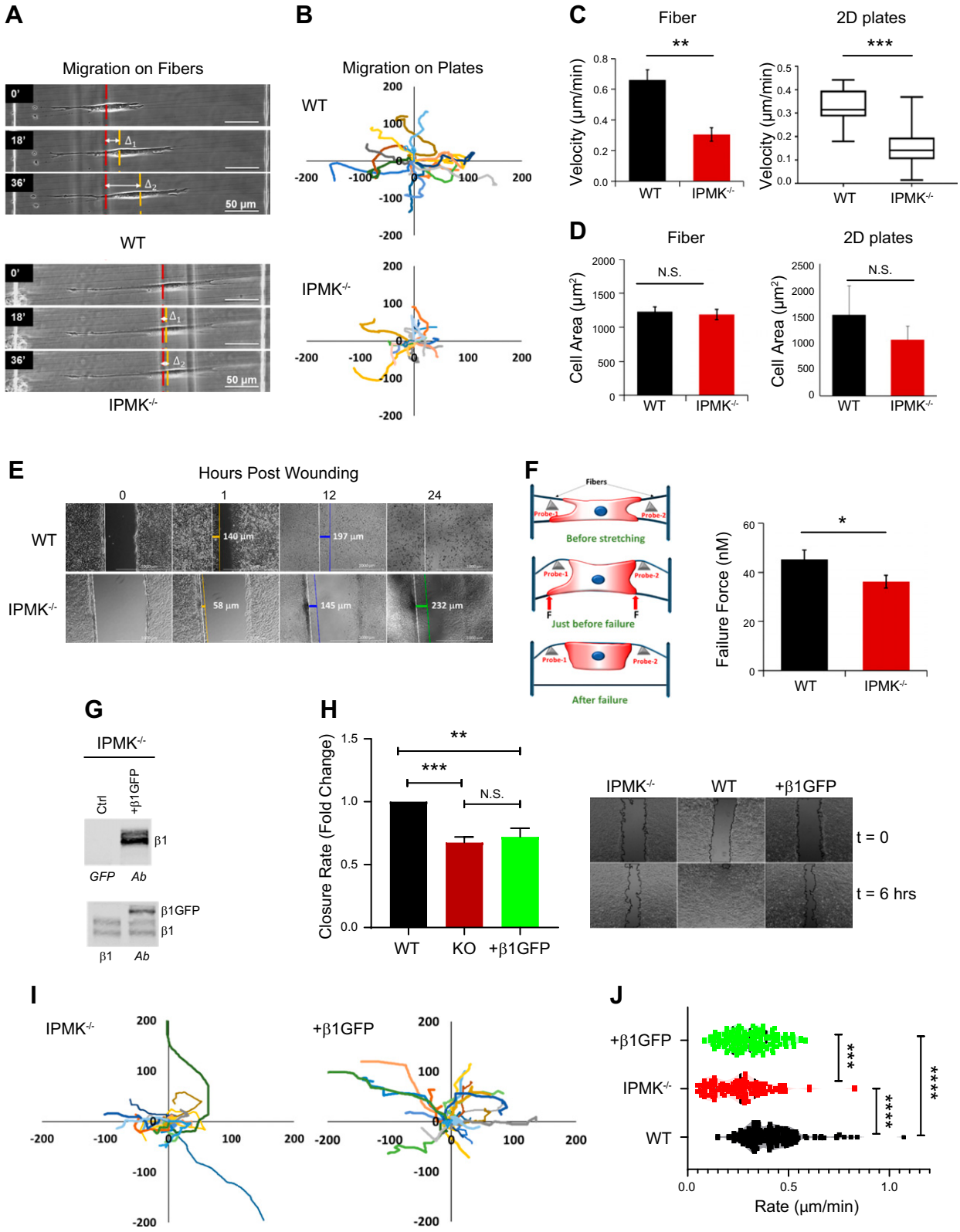

Figure 2. Loss of IPMK reduces cell migration. *A*) Time lapse images showing MEF WT migrating faster than IPMK$^{-/-}$ cells on aligned nanofibers. Red dashed line indicates starting position and yellow dashed line indicates the current location of the centroid of the cell at the indicated time. *B*) Cells were plated on fibronectin-coated MatTek glass-bottom plates as indicated in Materials and Methods and imaged at 2-min intervals. Individual cells were tracked using CellTracker v.1.1, and positions were normalized to the origin and are presented as rose plots. Results are representative of at least 3 experiments tracking 40–50 cells for each cell type. *C*) Quantification of velocity data from *A* and *B*. Fiber scaffold experiments are averaged data from 20 cells (error bars = SE); 2D experiments are averaged data from 40 to 50 cells. *D*) Quantification of cell area data from *A* and *B*. Fiber scaffold experiments are averaged data from 20 cells (error bars = SE); 2D experiments are averaged data from 100 cells. N.S., not

(*continued on next page*)

Briefly, force vectors were assigned along the dominant stress fibers originating from the focal adhesion clusters at either end of the cell-fiber attachment points; the total force exerted is the sum of the magnitude of these force vectors. Outside-in force experiments were performed by placing dual probes made from glass micropipettes mounted on a MP-285 motorized manipulator (Sutter Instruments, Novato, CA, USA). The probes were centered around a parallel-shaped cell stretched between 2 fibers. The top fiber was stretched by probes until the cell broke contact with the underside of the fiber. Only the vertical component of forces is considered for this force calculation (34, 35). For detailed information on the force calculations, see Computing Cell Force in the Supplemental Data.

Statistical analysis

Prism software (GraphPad, La Jolla, CA, USA) was used to test sample populations for statistical significance using the unpaired, 2-tailed Student's t test for comparisons between 2 groups, and the 1-way ANOVA test for multiple group comparisons. A value of $P \leq 0.05$ was used. Error bars represent SD unless noted otherwise.

RESULTS

Loss of IPMK reduces cell adhesion

Metformin treatment is known to interfere with cellular migration and to modulate IPMK protein levels, which led us to speculate that IPMK may regulate cellular migration in response to energy stress. To test this hypothesis, we treated MEFs with 2 mM metformin for 48 h and measured the level of IPMK. We observed a significant decrease in IPMK protein that was accompanied by expected metformin-induced increases in phosphorylated (p)AMPK and phosphorylated acetyl-CoA carboxylase (pACC), an AMPK target protein (**Fig. 1*A***). Based on published reports describing the disruption of cell:ECM adhesion by changes in inositol polyphosphates, we examined the level of the most ubiquitous integrin protein, integrin β1, under the same conditions and observed a similar decrease in protein level (Fig. 1*B*). To investigate the possibility of a causal link between IPMK loss and integrin β1 expression, we acutely deleted IPMK in primary myocytes, adipocytes, and hepatocytes isolated from IPMK loxp/loxp mice by treatment with adeno-Cre virus. IPMK knockdown decreased integrin β1 by ~50% in all cells tested, suggesting a general requirement for IPMK in maintaining integrin β1 levels (Supplemental Fig. S1).

To probe the functional consequence of decreased integrin, we turned to MEFs stably depleted of IPMK ($IPMK^{-/-}$), and found decreased levels of total and active integrin β1 (Fig. 1*C*). $IPMK^{-/-}$ cells incubated in calcium- and magnesium-free PBS rapidly detached from culture dishes during a brief (5 min) incubation period (Fig. 1*D*), and classification of fixed cell morphology revealed that $IPMK^{-/-}$ cells had a lower proportion of cells with broad lamellae (semicircular) and an increased proportion of cells with finger-like protrusions (spiky) (Fig. 1*E*). Because the formation of lamellar sheets are strongly associated with cell movement, we examined the effects of IPMK on cell migration. We followed migration by tracking individual cells over a 6-h period using 2 systems: standard tissue culture plates and suspended fiber networks. Nanonet fiber scaffolds mimic the ECM environment more closely than stiff plastic surfaces and have been shown to be an effective tool for measuring outside-in and inside-out cellular forces using NFM (34, 35). We found that $IPMK^{-/-}$ cells migrated more slowly than WT cells in both systems (**Fig. 2*A*, *C*** and Supplemental Movies S1 and S2). Overlays of cell tracks from migrating cells on tissue culture plates revealed that the migration paths for $IPMK^{-/-}$ cells were more contracted than those of WT cells (Fig. 2*B*), which is consistent with both a slower rate of movement and an increase in the number of turns (meandering or loss of persistence). To identify contributions of directionality to the path geometry, we compared directional persistence (DiPer) ratios for each cell tracked. DiPer is defined as the ratio of the final distance of a migrating cell from the path origin to the total path length traveled, and although this is a low-resolution metric, it is useful for identifying changes in the tendency for a cell to persist along a straight path. DiPer values were lower for $IPMK^{-/-}$ cells relative to WT cells (Supplemental Fig. S2), suggesting that loss of IPMK increases meandering behavior. In addition, individual $IPMK^{-/-}$ cells displayed a reduced migration rate (Fig. 2*C*) and a reduced surface area in both 2D and fiber-based cultures (Fig. 2*D*), which is consistent with integrin loss. Finally, in a cellular wound-healing assay, $IPMK^{-/-}$ cells had a slower rate of wound closure, indicating that the migration defect observed in single cells was also detectable in a population setting (Fig. 2*E*). Because integrin β1 is a major adhesion receptor, we next measured cell-matrix adhesion forces using NFM to determine the magnitude of change. Cells seeded onto fibronectin-coated nanonet fibers were allowed to adhere for 2 h, then the force required to detach

statistically significant. *E*) MEF cells were grown in 12-well plates and manually scratched with a pipette tip. Cell images were taken at indicated times, and the cell front is marked by a white line, whereas the migration progress is indicated by a colored line (orange = 6 h, blue = 12 h, green = 24 h). The distance traveled between 2 time points was measured using ImageJ and is indicated in each panel. No measurement indicates gap closure. *F*) Schematic representation of the pull to failure experiments to measure adhesion strength. MEF $IPMK^{-/-}$ cells have significantly lower adhesion strength compared with MEF WT cells; n = 14 for WT and n = 16 for $IPMK^{-/-}$. *G*) Integrin β1 was overexpressed in MEF $IPMK^{-/-}$ cells and its expression was confirmed by immunoblotting. *H*) Scratch assays were performed as described in *E*, and cells were imaged every 5 min for 4–8 h as indicated in Materials and Methods. Gap closure rates were determined normalized to WT controls. Combined data from 4 experiments; n = 14 for each cell type. *I*) Rose plots of cell tracking data from $IPMK^{-/-}$ and $IPMK^{-/-}$ cells stably expressing β1 integrin-GFP as described in *B*. Representative of 2 experiments, n = 50 cells for each cell type. *J*) Violin plot showing the distribution density of migration velocities for WT (black), $IPMK^{-/-}$ (red), and $IPMK^{-/-}$ + β1GFP (green) shows that IPMK loss decreases migration velocity, which is partially rescued by addback of integrin β1; n = 42–58 cells for each cell type. Combined data from 3 experiments. Ns, not significant. $^{*}P < 0.05$, $^{**}P < 0.01$, $^{***}P < 0.001$.

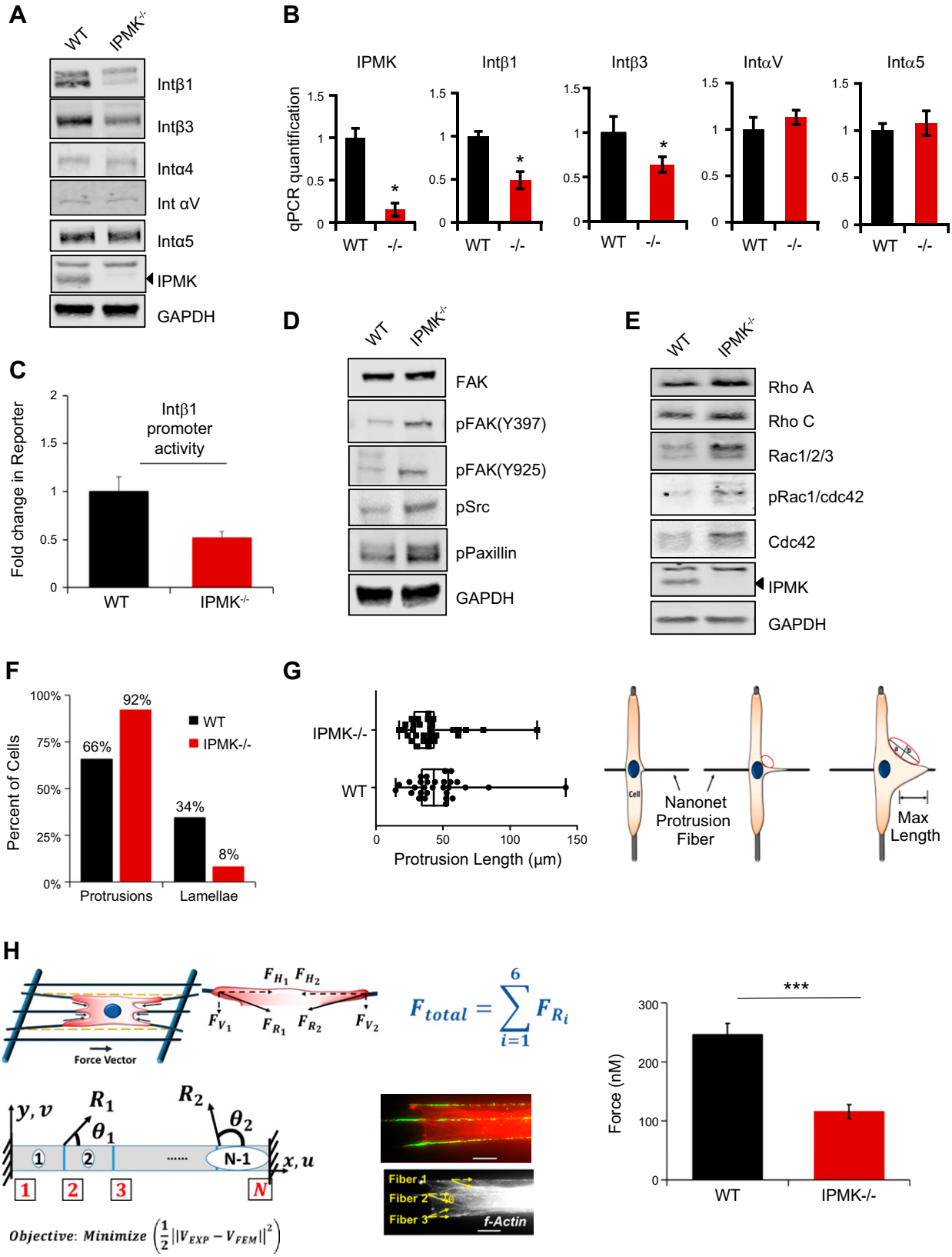

Figure 3. IPMK regulates the adhesion signaling network. *A*). MEF cells were harvested and cell lysates were subjected to immunoblotting. *B*) Expression of various adhesion molecule mRNA was detected by real-time qPCR. Data were pooled from at least 6 independent determinations, each in triplicate. *C*) A luciferase construct containing integrin (Int)β1 promoter region was expressed in either WT or IPMK$^{-/-}$ MEF cells, and a luciferase reporter assay was performed. Data were pooled from at least 3 independent determinations, each in triplicate. *D*, *E*) Immunoblotting was performed on cell lysates. *F*) The proportion of finger-like protrusions increases while the number of broad lamellae decrease in IPMK$^{-/-}$ cells; $n = 67$ cells for each cell type. *G*)

(*continued on next page*)

cells from fibers was determined to provide a quantitative measure of cell-matrix interaction strength. As expected, IPMK$^{-/-}$ cells detached at lower forces than WT cells (Fig. 2*F* and Supplemental Movie S3).

To determine whether the observed effects on migration were solely a consequence of the decreased level of integrin β1, we created a stable IPMK$^{-/-}$ cell line expressing integrin β1-GFP (+β1GFP) (Fig. 2*G*) and examined the effect on the migration rate in a wound healing assay. Although addback of integrin β1-GFP returned DiPer values to WT levels (Fig. 2*I* and Supplemental Fig. S2), it only had a minor effect on cell velocity (Fig. 2*J*) and no significant effect on wound closure rates (Fig. 2*H*).

Integrin expression is transcriptionally down-regulated following loss of IPMK activity

One explanation for the inability of exogenous integrin β1 to restore migration rates is that additional integrins might also be down-regulated. We examined the expression levels of 4 additional integrin isoforms: β3, α4, α5, and αv. We found that integrin β3 was also reduced compared with WT cells (**Fig. 3*A, B***). Using real-time quantitative PCR (qPCR) we established that both integrins β1 and β3 were reduced at the transcriptional level (Fig. 3*B*), whereas an integrin β1 promoter reporter assay showed a 50% reduction in promoter activity in IPMK$^{-/-}$ cells (Fig. 3*C*).

To evaluate signaling downstream of integrin β1, we measured the levels of FAK Y397 phosphorylation, a common readout for integrin activation, and Rho protein levels by Western blot. Phosphorylation of FAK typically occurs following engagement of integrin receptors, and the role of Rho family proteins in migration and cellular contractility is well established. Cellular and animal models depleted of integrin β1 exhibit reduced FAK activation (36). Unexpectedly, we found that pFAK (Y397, Y925) and its downstream targets, including pSrc and pPaxillin, were elevated in IPMK$^{-/-}$ cells (Fig. 3*D* and Supplemental Fig. S3) as were RhoA, Rac1/2/3, and Cdc42 protein levels (Fig. 3*E* and Supplemental Fig. S3). To examine potential consequences of FAK/Rho GTPase disruption, we evaluated the formation of membrane protrusions of WT and IPMK$^{-/-}$ fixed cells in 2D culture and in live cells seeded on nanonet protrusion scaffolds. Protrusion scaffolds consist of 2 fibers of different diameters deposited orthogonally on top of each other and fused at the intersections. This setup constrains cell migration to the larger-diameter base fiber (~2 μm) while allowing protrusions to sense and mature on smaller-diameter protrusive fibers, effectively decoupling the protrusions from the direction of migration (37). We found that IPMK$^{-/-}$ cells have a significant reduction in the number of cells with broad lamellae though >90% of cells exhibited thin protrusions in standard 2D culture (Fig. 3*F*). Live cell studies of protrusion growth on nanonet fibers suggest that IPMK$^{-/-}$ cells tend to extend shorter protrusions than WT cells, though no significant difference in average protrusion length was evident (Fig. 3*G*). RhoA plays a dominant role in promoting cell contractility by stimulating myosin light chain phosphorylation to promote actomyosin assembly, whereas Rac and Cdc42 inhibit contractility by inactivating myosin light chain kinase. To investigate IPMK contributions to cellular contractile forces, we measured fiber deflection exerted by migrating cells using NFM (see Supplemental Data for model details). Cumulative contractile forces were significantly higher for WT cells (Fig. 3*H*), indicating that IPMK contributes to cellular contractility. Importantly, we found no apparent defect in the size or number of focal adhesions (Supplemental Fig. S5*A, B*) indicating there is no gross change in the formation of adhesion complexes and potential anchor points.

IPMK activity regulates integrin β1 gene expression through FAK

We examined the activity dependence of IPMK on integrin β1 expression and FAK activation by comparing MEF IPMK$^{-/-}$ cells stably expressing myc-tagged WT IPMK (+WT) or kinase dead IPMK (+KD). We found that addback of active IPMK, but not inactive IPMK, restored integrin β1 and β3 levels, indicating the requirement for catalytic activity (**Fig. 4*A*** and Supplemental Fig. S4). This result was confirmed using RT-PCR, which showed an ~1.5-fold increase in integrin β1 mRNA levels for +WT cells (Fig. 4*B*). Furthermore, only addback of active IPMK decreased pFAK Y397 activation and Rho protein levels in IPMK$^{-/-}$ cells (Fig. 4*A* and Supplemental Fig. S4). The functional recovery of integrin β1 was examined using detachment and wound closure assays, which showed that addback of active IPMK (+WT) increased adhesion and accelerated gap closure rates relative to IPMK$^{-/-}$ cells, whereas addback of kinase dead IPMK (+KD) had no effect (Fig. 4*C* and Supplemental Movies S4 and S5). These data confirm that IPMK activity is required for proper functioning of the integrin β1/FAK/Rho axis in MEF cells.

The observed increase in FAK activation was unexpected and suggested the possible involvement of FAK in β1 gene regulation. To test this theory, we treated cells with 2 well-characterized FAK inhibitors—PF573,228 and PF431,396 (38, 39)—to determine the effect on integrin β1 gene expression. Overnight treatment with 2 μM of either

Mature protrusion length in WT and IPMK$^{-/-}$ cells extending onto 500-nM round nanofibers; $n = 30$ for each cell type (error bars = SE). Cartoon representation illustrates cells extending protrusions on fibers. The center of the ellipse denotes the base of the protrusion. *H*) Schematic representation of contractile forces measured using NFM. The forces reported here are the sum of the magnitudes of all the resultant force vectors. The force vectors are directed along the major stress fiber angles as shown by immunofluorescent images; red denotes f-actin and green denotes paxillin. Scale bars, 10 μm. MEF IPMK$^{-/-}$ cells had statistically significant lower forces than MEF WT cells; $n = 22$ for WT and $n = 14$ for IPMK$^{-/-}$ cells (error bars = SE). The most representative images from at least 5 independent assays are presented. $^*P < 0.05$.

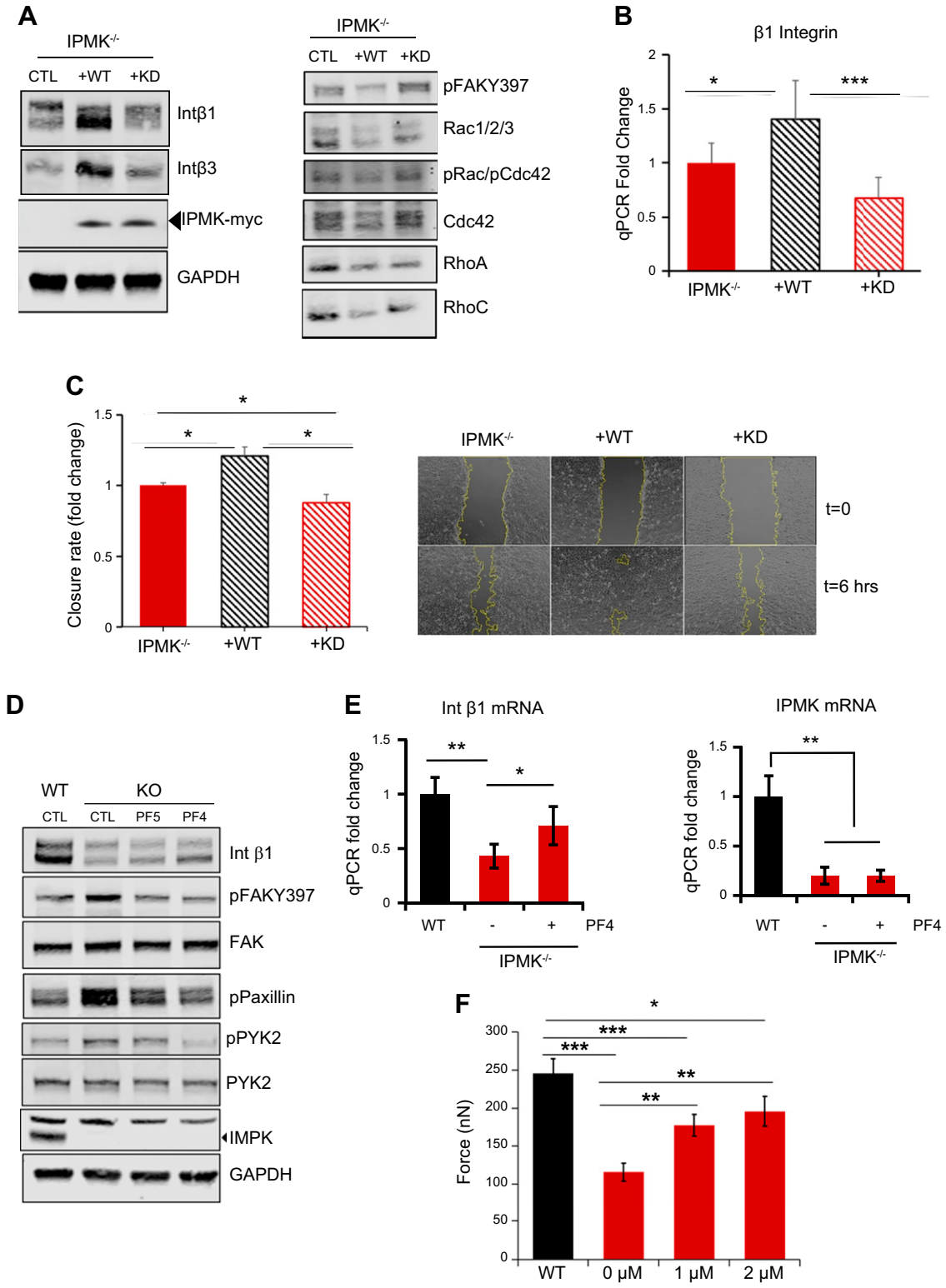

Figure 4. IPMK activity promotes integrin (Int)β1 expression *via* FAK. *A*) MEF IPMK$^{-/-}$ cells were overexpressed with either WT or inactive (kinase dead, KD) IPMK, and cell lysates were subjected to immunoblotting. *B*) Expression of integrin β1 mRNA was detected by real-time quantitative PCR (qPCR). *C*) Scratch assay was performed as described for Fig. 2*H*, and data were pooled from 4 experiments. *D*, *E*) Cells were treated with the indicated drugs (2 μM) for 18 h. Protein expression was examined by immunoblotting (*D*) and mRNA expression by qRT-PCR (*E*). *F*) The most representative Western blot images from at least 4 independent assays are presented, and qRT-PCR data were pooled from 6 independent determinations, each in triplicate. Contractile force measurements conducted using NFM show a dose-dependent increase in the inside-out forces for IPMK$^{-/-}$ cells following addition of PF431,396 (error bars = SE); $n = 22$ for WT control, $n = 14$ for IPMK$^{-/-}$ control, $n = 24$ for 1 μM, and $n = 14$ for 2 μM. $^{*}P < 0.05$, $^{**}P < 0.01$, $^{***}P < 0.001$.

inhibitor completely blocked FAK(Y397) phosphorylation, whereas only PF431,396 inhibited Pyk2(Y402) phosphorylation under these conditions. Notably, PF431,396 increased endogenous integrin β1 expression while PF573,228 had minimal effect (Fig. 4*D* and Supplemental Figs. S4 and S6). RT-PCR confirmed that 24 h of PF431,396 treatment increased integrin β1 mRNA levels almost 2-fold in IPMK$^{-/-}$ cells (Fig. 4*E*), and NFM measurement of contractile forces showed a dose-dependent increase in force after overnight treatment of cells with PF431,396 (Fig. 4*F*). Together, these data indicate that IPMK regulates FAK activity and suggests a negative feedback loop whereby sustained activation of the FAK/Pyk2 axis modulates cell migration by down-regulating β1 integrin gene expression.

DISCUSSION

In this study we show that short (24–48 h) treatment with metformin, a drug commonly used to treat diabetes, results in decreased levels of both IPMK and integrin β1 protein and defects in migration. Knockdown of IPMK in murine primary cultures of hepatocytes, myocytes, and adipoctyes and cultured MEF cells also resulted in loss of integrin β1, indicating a role for IPMK in integrin gene expression and suggesting loss of IPMK as the mechanism for metformin-induced loss of integrin β1. Contrary to expectations, the decrease in integrin β1 was accompanied by increased FAK activity as well as increased levels of RhoA, Rac, and Cdc42 protein. Both integrin β1 gene expression and FAK signaling were restored by addback of active IPMK but not by catalytically inactive IPMK, indicating that requirement for kinase activity. Together these data reveal a previously unknown regulatory function for IPMK in migration and mechanotransduction.

IPMK impacts both soluble and lipid-based phosphoinositols, impacting downstream signaling through IP6 kinases as well as regional levels of PIP_2 and PIP_3. IPMK activity is required for the production of the IP6K substrates [myo-inositol pentakisphosphate (IP5) and myo-inositol hexakisphosphate (IP6)], and in IPMK$^{-/-}$ MEF cells, IP5 is undetectable while IP6 is decreased by almost 90% (2, 24). Since previous reports on IP6-kinase-null cells (IP6K1 and IP6K2 isoforms) also exhibit defects in cell migration, we expected similar defects to be apparent following IPMK deletion, but our data indicate important distinctions. For example, in contrast to IPMK loss, IP6K1 knockdown increases cell-matrix adhesion (14), whereas IPMK loss decreases it. Loss of either IP6K1 or IP6K2 results in decreased pFAK levels, though by different proposed mechanisms. IP6K1-produced IP7 promotes FAK activation (40), whereas IP6K2 produces nuclear IP7 that prevents LKB1 translocation to the cytosol, where it appears to inhibit tyrosine phosphatases, thus preventing dephosphorylation of FAK1 (41). Contrary to this, IPMK loss increases FAK phosphorylation. Together our data indicate that IPMK regulation of FAK is upstream of the IP6 kinases and supports the importance of FAK regulation by inositol signaling.

We were intrigued to find that inhibition of the FAK axis promoted integrin β1 gene expression in IPMK$^{-/-}$ cells. The dual FAK1/Pyk2 inhibitor PF431,396 increased β1 gene expression after 24 h of treatment at a relatively low dose while the more specific FAK1-specific inhibitor PF573,228 only induced β1 expression at very high doses that also inhibit Pyk2, suggesting either that Pyk2 is the relevant target or that both FAK isoforms must be blocked to restore β1 expression and restore cell contractility. This finding is of particular interest since Pyk2 is activated by calcium, and loss of IPMK has been associated with an increase in inositol-3 phosphate (23), which promotes calcium release from internal stores. In addition, Pyk2 has been shown to directly phosphorylate FAK1 (42), and an increase in active Pyk2 is consistent with the high basal level of FAK(Y397) observed in IPMK$^{-/-}$ cells. Although Pyk2 is most highly expressed in nerve and hematopoietic cells, it has been shown to be active in fibroblasts, adipocytes, and myocytes (43), which all exhibit a decrease in integrin β1 following IPMK deletion (Fig. 3*A* and Supplemental Fig. S1).

We have previously shown an inverse relationship between AMPK activation and IPMK expression (1) and now report that one of the most widely used diabetes drugs, metformin, reduces the expression of IPMK, leading to impaired cell adhesion and migration. Indeed, numerous studies have evaluated metformin as a potential anticancer drug and demonstrated that it can reduce tumor cell proliferation and invasion with significantly fewer toxic effects than many other chemotherapeutic agents currently in use. This antimigratory effect may in part account for the recent reports that metformin does not improve wound healing as cell migration is one of the key aspects of the wound healing process (10). This is particularly relevant in light of the finding that IPMK loss is inducible by metformin treatment and leads to defects in adhesion and migration. Based on these findings, IPMK may be a suitable biomarker for the prognosis of wound healing outcome among diabetes patients. In summary, our study demonstrates that IPMK impacts cellular adhesion and integrin-based signaling, revealing a connection between energy status and cell migration. FJ

ACKNOWLEDGMENTS

The authors thank Jade West for assisting with cell tracking analyses, and Angie Chan for assisting with quantitative RT-PCR experiments (both from Johns Hopkins University). This work was supported by U.S. National Institutes of Health (NIH) Grant DA568921 (to S.F.K.), American Heart Association Grant 17SFRN33610014 (to S.F.K.), and National Science Foundation (NSF) Grants 1437101 and 1462916 (to A.N.). The authors declare no conflicts of interest.

AUTHOR CONTRIBUTIONS

B. Tu-Sekine, A. Nain, and S. F. Kim designed research; B. Tu-Sekine, S. Jin, and S. F. Kim performed research and analyzed data; S. Kalyan and S. C. Hur contributed analytic tools; A. Padhi, K. Singh, R. Kapania, and A. Nain developed the force model; A. Padhi, M. Apperson, and A. Nain analyzed force data; and B. Tu-Sekine, A. Nain, and S. F. Kim wrote the manuscript.

REFERENCES

1. Bang, S., Kim, S., Dailey, M. J., Chen, Y., Moran, T. H., Snyder, S. H., and Kim, S. F. (2012) AMP-activated protein kinase is physiologically regulated by inositol polyphosphate multikinase. *Proc. Natl. Acad. Sci. USA* **109**, 616–620
2. Bang, S., Chen, Y., Ahima, R. S., and Kim, S. F. (2014) Convergence of IPMK and LKB1-AMPK signaling pathways on metformin action. *Mol. Endocrinol.* **28**, 1186–1193
3. Kim, S., Kim, S. F., Maag, D., Maxwell, M. J., Resnick, A. C., Juluri, K. R., Chakraborty, A., Koldobskiy, M. A., Cha, S. H., Barrow, R., Snowman, A. M., and Snyder, S. H. (2011) Amino acid signaling to mTOR mediated by inositol polyphosphate multikinase. *Cell Metab.* **13**, 215–221
4. Arnold, S. E., Lucki, I., Brookshire, B. R., Carlson, G. C., Browne, C. A., Kazi, H., Bang, S., Choi, B. R., Chen, Y., McMullen, M. F., and Kim, S. F. (2014) High fat diet produces brain insulin resistance, synaptodendritic abnormalities and altered behavior in mice. *Neurobiol. Dis.* **67**, 79–87
5. Schexnayder, C., Broussard, K., Onuaguluchi, D., Poché, A., Ismail, M., McAtee, L.F., Llopis, S., Keizerweerd, A., McFerrin, H., and Williams, C. (2018) Metformin inhibits migration and invasion by suppressing ROS production and COX2 expression in MDA-MB-231 breast cancer cells. *Int. J. Mol. Sci.* **19**, 1–13
6. Yi, Y., Chen, D., Ao, J., Sun, S., Wu, M., Li, X., Bergholz, J., Zhang, Y., and Xiao, Z. X. (2017) Metformin promotes AMP-activated protein kinaseindependent suppression of δnp63α protein expression and inhibits cancer cell viability. *J. Biol. Chem.* **292**, 5253–5261
7. Qiang, P., Shao, Y., Sun, Y. P., Zhang, J., and Chen, L. J. (2019) Metformin inhibits proliferation and migration of endometrial cancer cells through regulating PI3K/AKT/MDM2 pathway. *Eur. Rev. Med. Pharmacol. Sci.* **23**, 1778–1785
8. Jang, S. Y., Kim, A., Kim, J. K., Kim, C., Cho, Y. H., Kim, J. H., Kim, C. H., and Lee, J. Y. (2014) Metformin inhibits tumor cell migration via down-regulation of MMP9 in tamoxifen-resistant breast cancer cells. *Anticancer Res.* **34**, 4127–4134
9. Yu, T., Wang, C., Yang, J., Guo, Y., Wu, Y., and Li, X. (2017) Metformin inhibits SUV39H1-mediated migration of prostate cancer cells. *Oncogenesis* **6**, e324
10. Ochoa-Gonzalez, F., Cervantes-Villagrana, A. R., Fernandez-Ruiz, J. C., Nava-Ramirez, H. S., Hernandez-Correa, A. C., Enciso-Moreno, J. A., and Castañeda-Delgado, J. E. (2016) Metformin induces cell cycle arrest, reduced proliferation, wound healing impairment in vivo and is associated to clinical outcomes in diabetic foot ulcer patients. *PLoS One* **11**, e0150900
11. Fesseha, B. K., Abularrage, C. J., Hines, K. F., Sherman, R., Frost, P., Langan, S., Canner, J., Likes, K. C., Hosseini, S. M., Jack, G., Hicks, C. W., Yalamanchi, S., and Mathioudakis, N. (2018) Association of hemoglobin A_{1c} and wound healing in diabetic foot ulcers. *Diabetes Care* **41**, 1478–1485
12. Reig, G., Pulgar, E., and Concha, M. L. (2014) Cell migration: from tissue culture to embryos. *Development* **141**, 1999–2013
13. Lamouille, S., Xu, J., and Derynck, R. (2014) Molecular mechanisms of epithelial-mesenchymal transition. *Nat. Rev. Mol. Cell Biol.* **15**, 178–196
14. Jadav, R. S., Kumar, D., Buwa, N., Ganguli, S., Thampatty, S. R., Balasubramanian, N., and Bhandari, R. (2016) Deletion of inositol hexakisphosphate kinase 1 (IP6K1) reduces cell migration and invasion, conferring protection from aerodigestive tract carcinoma in mice. *Cell. Signal.* **28**, 1124–1136
15. Insall, R. H., and Weiner, O. D. (2001) PIP3, PIP2, and cell movement–similar messages, different meanings? *Dev. Cell* **1**, 743–747
16. Welf, E. S., Ahmed, S., Johnson, H. E., Melvin, A. T., and Haugh, J. M. (2012) Migrating fibroblasts reorient directionality by a metastable, PI3K-dependent mechanism. *J. Cell Biol.* **197**, 105–114
17. Burridge, K., and Fath, K. (1989) Focal contacts: transmembrane links between the extracellular matrix and the cytoskeleton. *BioEssays* **10**, 104–108
18. Giancotti, F. G., and Ruoslahti, E. (1999) Integrin signaling. *Science* **285**, 1028–1032
19. Kim, C., Ye, F., and Ginsberg, M. H. (2011) Regulation of integrin activation. *Annu. Rev. Cell Dev. Biol.* **27**, 321–345
20. Hynes, R. O. (2002) Integrins: bidirectional, allosteric signaling machines. *Cell* **110**, 673–687
21. Barczyk, M., Carracedo, S., and Gullberg, D. (2010) Integrins. *Cell Tissue Res.* **339**, 269–280
22. Koivisto, L., Heino, J., Häkkinen, L., and Larjava, H. (2014) Integrins in wound healing. *Adv. Wound Care (New Rochelle)* **3**, 762–783
23. Resnick, A. C., Snowman, A. M., Kang, B. N., Hurt, K. J., Snyder, S. H., and Saiardi, A. (2005) Inositol polyphosphate multikinase is a nuclear PI3-kinase with transcriptional regulatory activity. *Proc. Natl. Acad. Sci. USA* **102**, 12783–12788
24. Maag, D., Maxwell, M. J., Hardesty, D. A., Boucher, K. L., Choudhari, N., Hanno, A. G., Ma, J. F., Snowman, A. S., Pietropaoli, J. W., Xu, R., Storm, P. B., Saiardi, A., Snyder, S. H., and Resnick, A. C. (2011) Inositol polyphosphate multikinase is a physiologic PI3-kinase that activates Akt/PKB. *Proc. Natl. Acad. Sci. USA* **108**, 1391–1396
25. Xu, R., Paul, B. D., Smith, D. R., Tyagi, R., Rao, F., Khan, A. B., Blech, D. J., Vandiver, M. S., Harraz, M. M., Guha, P., Ahmed, I., Sen, N., Gallagher, M., and Snyder, S. H. (2013) Inositol polyphosphate multikinase is a transcriptional coactivator required for immediate early gene induction. *Proc. Natl. Acad. Sci. USA* **110**, 16181–16186
26. Malabanan, M. M., and Blind, R. D. (2016) Inositol polyphosphate multikinase (IPMK) in transcriptional regulation and nuclear inositide metabolism. *Biochem. Soc. Trans.* **44**, 279–285
27. Parsons, M., Messent, A. J., Humphries, J. D., Deakin, N. O., and Humphries, M. J. (2008) Quantification of integrin receptor agonism by fluorescence lifetime imaging. *J. Cell Sci.* **121**, 265–271
28. Han, S. J., Choi, S. E., Yi, S. A., Jung, J. G., Jung, I. R., Shin, M., Kang, S., Oh, H., Kim, H. J., Kim, D. J., Kwon, J. E., Choi, C. S., Lee, K. W., and Kang, Y. (2016) Glutamate dehydrogenase activator BCH stimulating reductive amination prevents high fat/high fructose diet-induced steatohepatitis and hyperglycemia in C57BL/6J mice. *Sci. Rep.* **5**, 37468
29. Nain, A. S., Sitti, M., Jacobson, A., Kowalewski, T., and Amon, C. (2009) Dry spinning based spinneret based tunable engineered parameters (STEP) technique for controlled and aligned deposition of polymeric nanofibers. *Macromol. Rapid Commun.* **30**, 1406–1412
30. Nain, A. S., and Wang, J. (2013) Polymeric nanofibers: isodiametric design space and methodology for depositing aligned nanofiber arrays in single and multiple layers. *Polym. J.* **45**, 695–700
31. Chalfoun, J., Majurski, M., Blattner, T., Bhadriraju, K., Keyrouz, W., Bajcsy, P., and Brady, M. (2017) MIST: accurate and scalable microscopy image stitching tool with stage modeling and error minimization. *Sci. Rep.* **7**, 4988
32. Lowe, D. G. (2004) Distinctive image features from scale-invariant keypoints. *Int. J. Comput. Vis.* **60**, 91–110
33. Piccinini, F., Kiss, A., and Horvath, P. (2016) CellTracker (not only) for dummies. *Bioinformatics* **32**, 955–957
34. Sheets, K., Wang, J., Zhao, W., Kapania, R., and Nain, A. S. (2016) Nanonet force microscopy for measuring cell forces. *Biophys. J.* **111**, 197–207
35. Hall, A., Chan, P., Sheets, K., Apperson, M., Delaughter, C., Gleason, T. G., Phillippi, J. A., and Nain, A. (2017) Nanonet force microscopy for measuring forces in single smooth muscle cells of the human aorta. *Mol. Biol. Cell* **28**, 1894–1900
36. Hou, S., Isaji, T., Hang, Q., Im, S., Fukuda, T., and Gu, J. (2016) Distinct effects of β1 integrin on cell proliferation and cellular signaling in MDA-MB-231 breast cancer cells. *Sci. Rep.* **6**, 18430
37. Koons, B., Sharma, P., Ye, Z., Mukherjee, A., Lee, M. H., Wirtz, D., Behkam, B., and Nain, A. S. (2017) Cancer protrusions on a tightrope: nanofiber curvature contrast quantitates single protrusion dynamics. *ACS Nano* **11**, 12037–12048
38. Slack-Davis, J. K., Martin, K. H., Tilghman, R. W., Iwanicki, M., Ung, E. J., Autry, C., Luzzio, M. J., Cooper, B., Kath, J. C., Roberts, W. G., and Parsons, J. T. (2007) Cellular characterization of a novel focal adhesion kinase inhibitor. *J. Biol. Chem.* **282**, 14845–14852
39. Calalb, M. B., Polte, T. R., and Hanks, S. K. (1995) Tyrosine phosphorylation of focal adhesion kinase at sites in the catalytic domain regulates kinase activity: a role for Src family kinases. *Mol. Cell. Biol.* **15**, 954–963
40. Fu, C., Xu, J., Cheng, W., Rojas, T., Chin, A. C., Snowman, A. M., Harraz, M. M., and Snyder, S. H. (2017) Neuronal migration is mediated by inositol hexakisphosphate kinase 1 via α-actinin and focal adhesion kinase. *Proc. Natl. Acad. Sci. USA* **114**, 2036–2041
41. Scherer, P. C., Ding, Y., Liu, Z., Xu, J., Mao, H., Barrow, J. C., Wei, N., Zheng, N., Snyder, S. H., and Rao, F. (2016) Inositol hexakisphosphate (IP6) generated by IP5K mediates cullin-COP9 signalosome interactions and CRL function. *Proc. Natl. Acad. Sci. USA* **113**, 3503–3508
42. Li, X., Dy, R. C., Cance, W. G., Graves, L. M., and Earp, H. S. (1999) Interactions between two cytoskeleton-associated tyrosine kinases: calcium-dependent tyrosine kinase and focal adhesion tyrosine kinase. *J. Biol. Chem.* **274**, 8917–8924
43. Murphy, J. M., Park, H., and Lim, S.-T. (2016) {FAK} and Pyk2 in disease. *Front. Biol. (Beijing)* **11**, 1–9

Received for publication March 22, 2019.
Accepted for publication September 17, 2019.